$Revision: 1.22 $ Date: 12 March 2008

First application of a coherent algorithm for gravitational-wave burst detection to data acquired by laser interferometric detectors

B Abbott[1], R Abbott[1], R Adhikari[1], J Agresti[1], P Ajith[2], B Allen[2,3], R Amin[4], S B Anderson[1], W G Anderson[3], M Arain[5], M Araya[1], H Armandula[1], M Ashley[6], S Aston[7], P Aufmuth[8], C Aulbert[9], S Babak[9], S Ballmer[1], H Bantilan[10], B C Barish[1], C Barker[11], D Barker[11], B Barr[12], P Barriga[13], M A Barton[12], K Bayer[14], K Belczynski[15], J Betzwieser[14], P T Beyersdorf[16], B Bhawal[1], I A Bilenko[17], G Billingsley[1], R Biswas[3], E Black[1], K Blackburn[1], L Blackburn[14], D Blair[13], B Bland[11], J Bogenstahl[12], L Bogue[18], R Bork[1], V Boschi[1], S Bose[19], P R Brady[3], V B Braginsky[17], J E Brau[20], M Brinkmann[2], A Brooks[21], D A Brown[1,22], A Bullington[23], A Bunkowski[2], A Buonanno[24], O Burmeister[2], D Busby[1], R L Byer[23], L Cadonati[14], G Cagnoli[12], J B Camp[25], J Cannizzo[25], K Cannon[3], C A Cantley[12], J Cao[14], L Cardenas[1], M M Casey[12], G Castaldi[26], C Cepeda[1], E Chalkley[12], P Charlton[27], S Chatterji[1], S Chelkowski[2], Y Chen[9], F Chiadini[28], D Chin[29], E Chin[13], J Chow[6], N Christensen[10], J Clark[12], P Cochrane[2], T Cokelaer[30], C N Colacino[7], R Coldwell[5], R Conte[28], D Cook[11], T Corbitt[14], D Coward[13], D Coyne[1], J D E Creighton[3], T D Creighton[1], R P Croce[26], D R M Crooks[12], A M Cruise[7], A Cumming[12], J Dalrymple[31], E D'Ambrosio[1], K Danzmann[2,8], G Davies[30], D DeBra[23], J Degallaix[13], M Degree[23], T Demma[26], V Dergachev[29], S Desai[32], R DeSalvo[1], S Dhurandhar[33], M Díaz[34], J Dickson[6], A Di Credico[31],

G Diederichs[8], A Dietz[30], E E Doomes[35], R W P Drever[36], J.-C Dumas[13], R J Dupuis[1], J G Dwyer[37], P Ehrens[1], E Espinoza[1], T Etzel[1], M Evans[1], T Evans[18], S Fairhurst[1,30], Y Fan[13], D Fazi[1], M M Fejer[23], L S Finn[32], V Fiumara[28], N Fotopoulos[3], A Franzen[8], K Y Franzen[5], A Freise[7], R Frey[20], T Fricke[38], P Fritschel[14], V V Frolov[18], M Fyffe[18], V Galdi[26], J Garofoli[11], I Gholami[9], J A Giaime[4,18], S Giampanis[38], K D Giardina[18], K Goda[14], E Goetz[29], L M Goggin[1], G González[4], S Gossler[6], A Grant[12], S Gras[13], C Gray[11], M Gray[6], J Greenhalgh[39], A M Gretarsson[40], R Grosso[34], H Grote[2], S Grunewald[9], M Guenther[11], R Gustafson[29], B Hage[8], D Hammer[3], C Hanna[4], J Hanson[18], J Harms[2], G Harry[14], E Harstad[20], T Hayler[39], J Heefner[1], I S Heng[12], A Heptonstall[12], M Heurs[2], M Hewitson[2], S Hild[8], E Hirose[31], D Hoak[18], D Hosken[21], J Hough[12], E Howell[13], D Hoyland[7], S H Huttner[12], D Ingram[11], E Innerhofer[14], M Ito[20], Y Itoh[3], A Ivanov[1], D Jackrel[23], B Johnson[11], W W Johnson[4], D I Jones[41], G Jones[30], R Jones[12], L Ju[13], P Kalmus[37], V Kalogera[15], D Kasprzyk[7], E Katsavounidis[14], K Kawabe[11], S Kawamura[42], F Kawazoe[42], W Kells[1], D G Keppel[1], F Ya Khalili[17], C Kim[15], P King[1], J S Kissel[4], S Klimenko[5], K Kokeyama[42], V Kondrashov[1], R K Kopparapu[4], D Kozak[1], B Krishnan[9], P Kwee[8], P K Lam[6], M Landry[11], B Lantz[23], A Lazzarini[1], B Lee[13], M Lei[1], J Leiner[19], V Leonhardt[42], I Leonor[20], K Libbrecht[1], P Lindquist[1], N A Lockerbie[43], M Longo[28], M Lormand[18], M Lubinski[11], H Lück[2,8], B Machenschalk[9], M MacInnis[14], M Mageswaran[1], K Mailand[1], M Malec[8], V Mandic[1], S Marano[28], S Márka[37], J Markowitz[14], E Maros[1], I Martin[12], J N Marx[1], K Mason[14], L Matone[37], V Matta[28], N Mavalvala[14], R McCarthy[11], D E McClelland[6], S C McGuire[35], M McHugh[44], K McKenzie[6], J W C McNabb[32], S McWilliams[25], T Meier[8], A Melissinos[38], G Mendell[11], R A Mercer[5], S Meshkov[1], C J Messenger[12], D Meyers[1], E Mikhailov[14],

S Mitra[33], V P Mitrofanov[17], G Mitselmakher[5], R Mittleman[14], O Miyakawa[1], S Mohanty[34], G Moreno[11], K Mossavi[2], C MowLowry[6], A Moylan[6], D Mudge[21], G Mueller[5], S Mukherjee[34], H Müller-Ebhardt[2], J Munch[21], P Murray[12], E Myers[11], J Myers[11], T Nash[1], G Newton[12], A Nishizawa[42], K Numata[25], B O'Reilly[18], R O'Shaughnessy[15], D J Ottaway[14], H Overmier[18], B J Owen[32], Y Pan[24], M A Papa[3,9], V Parameshwaraiah[11], P Patel[1], M Pedraza[1], S Penn[45], V Pierro[26], I M Pinto[26], M Pitkin[12], H Pletsch[2], M V Plissi[12], F Postiglione[28], R Prix[9], V Quetschke[5], F Raab[11], D Rabeling[6], H Radkins[11], R Rahkola[20], N Rainer[2], M Rakhmanov[32], M Ramsunder[32], K Rawlins[14], S Ray-Majumder[3], V Re[7], H Rehbein[2], S Reid[12], D H Reitze[5], L Ribichini[2], R Riesen[18], K Riles[29], B Rivera[11], N A Robertson[1,12], C Robinson[30], E L Robinson[7], S Roddy[18], A Rodriguez[4], A M Rogan[19], J Rollins[37], J D Romano[30], J Romie[18], R Route[23], S Rowan[12], A Rüdiger[2], L Ruet[14], P Russell[1], K Ryan[11], S Sakata[42], M Samidi[1], L Sancho de la Jordana[46], V Sandberg[11], V Sannibale[1], S Saraf[47], P Sarin[14], B S Sathyaprakash[30], S Sato[42], P R Saulson[31], R Savage[11], P Savov[22], S Schediwy[13], R Schilling[2], R Schnabel[2], R Schofield[20], B F Schutz[9,30], P Schwinberg[11], S M Scott[6], A C Searle[6], B Sears[1], F Seifert[2], D Sellers[18], A S Sengupta[30], P Shawhan[24], D H Shoemaker[14], A Sibley[18], X Siemens[1,22], D Sigg[11], S Sinha[23], A M Sintes[9,46], B J J Slagmolen[6], J Slutsky[4], J R Smith[2], M R Smith[1], K Somiya[2,9], K A Strain[12], D M Strom[20], A Stuver[32], T Z Summerscales[48], K.-X Sun[23], M Sung[4], P J Sutton[1], H Takahashi[9], D B Tanner[5], M Tarallo[1], R Taylor[1], R Taylor[12], J Thacker[18], K A Thorne[32], K S Thorne[22], A Thüring[8], K V Tokmakov[12], C Torres[34], C Torrie[12], G Traylor[18], M Trias[46], W Tyler[1], D Ugolini[49], C Ungarelli[7], K Urbanek[23], H Vahlbruch[8], M Vallisneri[22], C Van Den Broeck[30], M Varvella[1], S Vass[1], A Vecchio[7], J Veitch[12], P Veitch[21], A Villar[1], C Vorvick[11],

S P Vyachanin[17], S J Waldman[1], L Wallace[1], H Ward[12], R Ward[1], K Watts[18], D Webber[1], A Weidner[2], M Weinert[2], A Weinstein[1], R Weiss[14], S Wen[4], K Wette[6], J T Whelan[9], D M Whitbeck[32], S E Whitcomb[1], B F Whiting[5], C Wilkinson[11], P A Willems[1], L Williams[5], B Willke[2,8], I Wilmut[39], W Winkler[2], C C Wipf[14], S Wise[5], A G Wiseman[3], G Woan[12], D Woods[3], R Wooley[18], J Worden[11], W Wu[5], I Yakushin[18], H Yamamoto[1], Z Yan[13], S Yoshida[50], N Yunes[32], M Zanolin[14], J Zhang[29], L Zhang[1], C Zhao[13], N Zotov[51], M Zucker[14], H zur Mühlen[8] and J Zweizig[1]

(LIGO Scientific Collaboration)

[1] LIGO - California Institute of Technology, Pasadena, CA 91125, USA
[2] Albert-Einstein-Institut, Max-Planck-Institut für Gravitationsphysik, D-30167 Hannover, Germany
[3] University of Wisconsin-Milwaukee, Milwaukee, WI 53201, USA
[4] Louisiana State University, Baton Rouge, LA 70803, USA
[5] University of Florida, Gainesville, FL 32611, USA
[6] Australian National University, Canberra, 0200, Australia
[7] University of Birmingham, Birmingham, B15 2TT, United Kingdom
[8] Leibnitz Universität Hannover, D-30167 Hannover, Germany
[9] Albert-Einstein-Institut, Max-Planck-Institut für Gravitationsphysik, D-14476 Golm, Germany
[10] Carleton College, Northfield, MN 55057, USA
[11] LIGO Hanford Observatory, Richland, WA 99352, USA
[12] University of Glasgow, Glasgow, G12 8QQ, United Kingdom
[13] University of Western Australia, Crawley, WA 6009, Australia
[14] LIGO - Massachusetts Institute of Technology, Cambridge, MA 02139, USA
[15] Northwestern University, Evanston, IL 60208, USA
[16] San Jose State University, San Jose, CA 95192, USA
[17] Moscow State University, Moscow, 119992, Russia
[18] LIGO Livingston Observatory, Livingston, LA 70754, USA
[19] Washington State University, Pullman, WA 99164, USA
[20] University of Oregon, Eugene, OR 97403, USA
[21] University of Adelaide, Adelaide, SA 5005, Australia
[22] Caltech-CaRT, Pasadena, CA 91125, USA
[23] Stanford University, Stanford, CA 94305, USA
[24] University of Maryland, College Park, MD 20742 USA
[25] NASA/Goddard Space Flight Center, Greenbelt, MD 20771, USA
[26] University of Sannio at Benevento, I-82100 Benevento, Italy
[27] Charles Sturt University, Wagga Wagga, NSW 2678, Australia
[28] University of Salerno, 84084 Fisciano (Salerno), Italy

[29] University of Michigan, Ann Arbor, MI 48109, USA
[30] Cardiff University, Cardiff, CF24 3AA, United Kingdom
[31] Syracuse University, Syracuse, NY 13244, USA
[32] The Pennsylvania State University, University Park, PA 16802, USA
[33] Inter-University Centre for Astronomy and Astrophysics, Pune - 411007, India
[34] The University of Texas at Brownsville and Texas Southmost College, Brownsville, TX 78520, USA
[35] Southern University and A&M College, Baton Rouge, LA 70813, USA
[36] California Institute of Technology, Pasadena, CA 91125, USA
[37] Columbia University, New York, NY 10027, USA
[38] University of Rochester, Rochester, NY 14627, USA
[39] Rutherford Appleton Laboratory, Chilton, Didcot, Oxon OX11 0QX United Kingdom
[40] Embry-Riddle Aeronautical University, Prescott, AZ 86301 USA
[41] University of Southampton, Southampton, SO17 1BJ, United Kingdom
[42] National Astronomical Observatory of Japan, Tokyo 181-8588, Japan
[43] University of Strathclyde, Glasgow, G1 1XQ, United Kingdom
[44] Loyola University, New Orleans, LA 70118, USA
[45] Hobart and William Smith Colleges, Geneva, NY 14456, USA
[46] Universitat de les Illes Balears, E-07122 Palma de Mallorca, Spain
[47] Rochester Institute of Technology, Rochester, NY 14623, USA
[48] Andrews University, Berrien Springs, MI 49104 USA
[49] Trinity University, San Antonio, TX 78212, USA
[50] Southeastern Louisiana University, Hammond, LA 70402, USA
[51] Louisiana Tech University, Ruston, LA 71272, USA

AUTHORSHIP LIST NOT UP TO DATE

E-mail: `i.heng@physics.gla.ac.uk`

Abstract.
We present the results of the first joint search for gravitational-wave bursts by the LIGO and GEO 600 detectors. We search for bursts with characteristic central frequencies in the band 768 to 2048 Hz in the data acquired between the 22nd of February and the 23rd of March, 2005 (fourth LIGO Science Run - S4). We discuss the inclusion of the GEO 600 data in the Waveburst-CorrPower pipeline which first searches for coincident excess power events without taking into account differences in the antenna responses or strain sensitivities of the various detectors. We compare the performance of this pipeline to that of the coherent Waveburst pipeline based on the maximum likelihood statistic. This likelihood statistic is derived from a coherent sum of the detector data streams that takes into account the antenna patterns and sensitivities of the different detectors in the network. We find that the coherent Waveburst pipeline is sensitive to signals of amplitude $30-50\%$ smaller than the Waveburst-CorrPower

pipeline. We perform a search for gravitational-waves bursts using both pipelines and find no detection candidates in the S4 data set.

1. Introduction

The worldwide network of interferometric gravitational wave detectors currently includes the three detectors of LIGO [1], as well as the GEO 600 [2], Virgo [3] and TAMA300 [4] detectors. The LIGO and GEO 600 detectors and affiliated institutions form the LIGO Scientific Collaboration (LSC). The LSC has performed several joint operational runs of its detectors. During the course of the most recent runs, the detectors have reached sensitivities that may allow them to detect gravitational waves from distant astrophysical sources.

Expected sources of gravitational-wave bursts include, for example, core-collapse supernovae and the merger phase of inspiralling compact object binaries. In general, due to the complex physics involved in such systems, the waveforms of the gravitational wave signals are not well-modelled.

There are two broad categories of gravitational-wave bursts searches. *Triggered searches* use information from an external observation, such as a gamma-ray burst, to focus on a short time interval, permitting a relatively low threshold to be placed on signal-to-noise ratio (SNR) for a fixed false alarm probability. *All-sky searches* are designed to maximise the detection efficiency for gravitational-wave bursts across the entire sky for data acquired over the entire run (spanning weeks or months depending on the run) for a given false alarm probability.

Previous all-sky burst searches performed by the LSC typically consisted of a first stage which identifies coincident excess power in multiple detectors and a second stage which tests the consistency of the data with the presence of a gravitational wave signal [6, 7, 8, 9]. The Waveburst-CorrPower (WBCP) pipeline is a example of such a two stage analysis. The first stage, performed by Waveburst, involves a wavelet packet transformation of the data and identification of excess power in time-frequency volumes which are coincident between multiple detections [10]. A waveform consistency test is then performed by the CorrPower algorithm which quantifies how well the detected waveforms match each other by using the r-statistic [11, 12]. The approach has been used to search for gravitational-wave bursts by the LSC in data acquired during the second through fourth Science Runs.

One should note that this pipeline requires coincident excess power to be observed in all detectors in the network to trigger the waveform consistency

test performed by CorrPower. Furthermore, CorrPower works on the underlying assumption that all detectors in the network have similar responses to the same gravitational wave signal. This assumption is valid for the LIGO detectors, which have similar orientations and noise spectra. However, GEO 600 has a different orientation on the Earth (see Figure 1), so that the received signal in this detector is a different linear combination of the h_+ and $h_\times$ polarisations from that in the LIGO detectors. Furthermore, the GEO 600 noise spectrum during the fourth LSC Science Run, S4, (22nd of February to 23rd of March, 2005) was quite different from those of LIGO (see Figure 2), with best GEO 600 sensitivity around 1 kHz. As a consequence, the approximation of a common signal response breaks down for the LIGO-GEO network. For example, particularly low frequency, gravitational-wave burst may appear in LIGO but not be evident in GEO 600. Alternatively, a gravitational-wave burst may appear more strongly in GEO 600 than in LIGO if it is incident from a sky direction for which the GEO antenna response is significantly larger than those of the LIGO detectors. These effects complicate a coincidence analysis of the sort employed by the LSC in previous burst searches since the sensitivity of the network tends to be limited by the least sensitive detector [9].

Coherent burst search algorithms have been developed to fold in data from a network of detectors with different sensitivities and orientations. Methods for coherent burst searches were first described in [13] and [14]. In the first paper [13], Gürsel and Tinto have shown for a network of three detectors that a gravitational wave signal can be cancelled out by forming a particular linear combination of data from pairs of detectors in the network, producing what is commonly referred to as the null stream. Conversely, coincident instrumental or environmental transient artifacts (glitches) that are not consistent between the detectors will usually leave some residual signature in the null stream, which can be used as a powerful tool for rejection of glitches [15, 16]. In [14], Flanagan and Hughes describe a likelihood method for detection and reconstruction of two polarizations of a gravitational wave signal. A modified likelihood method [17] which uses model independent constraints imposed on the likelihood functional is used for implementation of the coherent Waveburst (cWB) algorithm [18]. It uses the maximum likelihood statistic, calculated for each point in the sky, which represents a total signal-to-noise ratio of the gravitational wave signal detected in the network.

In this article, we present the first burst search using data from the three LIGO detectors and GEO 600, acquired during the fourth Science Run of the LSC. We present a search for gravitational-wave bursts between 768 and 2048 Hz using both the Waveburst-CorrPower and coherent Waveburst pipelines. We

begin with a brief description of the detectors in section 2 before describing the two methods used to analyse the acquired data in section 3. We then detail the additional selection criteria and vetoes in section 4. We present the results of the search in section 5 and compare the detection efficiencies of the two methods. Finally, we discuss our observations in section 6.

2. Instruments and data

Here, we present a brief description of the main features of the LIGO and GEO 600 detectors. A more detailed description of the LIGO detectors in their S4 configuration can be found in [1]. The most recent description of the GEO 600 detector can be found in [2] and [19].

LIGO consists of three laser interferometric detectors at two locations in the United States of America. There are two detectors at the Hanford site, one with 4-km arms and another with 2-km arms, which we refer to as H1 and H2, respectively. In Livingston, there is one detector with 4-km arms which we refer to as L1. Each detector consists of a Michelson interferometer with Fabry-Perot cavities in both arms. The laser light power builds up in these resonant cavities, enhancing the sensitivity of the detector. At the input to the interferometer, there is a power-recycling mirror which increases the stored laser light power in the interferometer. This reduces the shot noise, allowing for better sensitivity at higher frequencies.

The GEO 600 laser interferometric gravitational wave detector (G1) has been built and operated by a British-German collaboration. It is located near Hannover in Germany and, along with the three LIGO detectors, is part of the LSC interferometer network. GEO 600 is a Michelson interferometer with 600-m arms. The optical path is folded once to give 2400 m round-trip length. To compensate for the shorter arm length, GEO 600 incorporates not only power-recycling, but also signal-recycling (SR), which allows the response of the interferometer to be shaped, and the frequency of maximum response to be chosen – the 'SR detuning' frequency. During the S4 run, a test power-recycling mirror with 1.35 % transmission was installed, yeilding an intra cavity power of only 500 W. As a result, the sensitivity of GEO 600 above 500 Hz was limited nearly entirely by shot noise [21]. The SR mirror had about 2 % transmission and the SR detuning frequency was set at 1 kHz. An overview of the signal processing and calibration process in S4 is given in [20].

The strain spectral densities of each detector during S4 is shown in Figure 2. GEO 600 achieved a duty factor of 96.5%, despite running in a fully automated

mode with minimal human interaction for operation and maintenance. H1, H2 and L1 achieved duty cycles of 80.5%, 81.4%, and 74.5% respectively.

The detected strain observed by each detector, $\xi(t)$, for a gravitational wave signal with strain amplitudes of $h_+(t)$ and $h_\times(t)$ in the plus and cross polarisations, respectively, is given by

$$\xi(t) = F_+(\alpha, \delta)h_+(t) + F_\times(\alpha, \delta)h_\times(t), \quad (1)$$

where $F_+(\alpha, \delta)$ and $F_\times(\alpha, \delta)$ are the antenna responses to the plus and cross polarisations. The antenna responses depend on the locations and orientations of the interferometers on the Earth's surface, where α and δ are the Greenwich hour angle and declination of the source in Earth-fixed coordinates [23].

Figure 1 shows the sum-squared antenna response $(F_+^2 + F_\times^2)$ for each site in the LIGO-GEO network in a fixed-Earth coordinate system. The Hanford and Livingston detectors are well aligned to each other and, therefore, have very similar antenna patterns. On the other hand, the GEO 600 detector has different antenna patterns, with peak sensitivities in sky locations that are near the minima of the LIGO detectors.

3. Search algorithms

In this section, we describe the two search pipelines used for the analysis. The WBCP pipeline is almost identical to that used to perform previous searches for gravitational-wave bursts [6, 7, 8]. However, for the analysis reported in this article, Waveburst is applied to data acquired by the LIGO and GEO 600 detectors, while CorrPower is applied only to data acquired by the LIGO detectors (see below for further explanation). The performance of the WBCP pipeline will be compared to that of the cWB pipeline. The same data were processed, using the two pipelines.

3.1. Waveburst and CorrPower pipeline

We give a brief description of the WBCP pipeline. More detailed descriptions of the Waveburst and CorrPower algorithms can be found in [10] and [11] respectively.

The data acquired by each detector in the network are processed by the Waveburst algorithm which performs a wavelet packet transformation using the Meyer wavelet [22]. This creates a time-frequency (TF) map of the data. A threshold is applied to this map to pick out TF volumes or *pixels* with significant

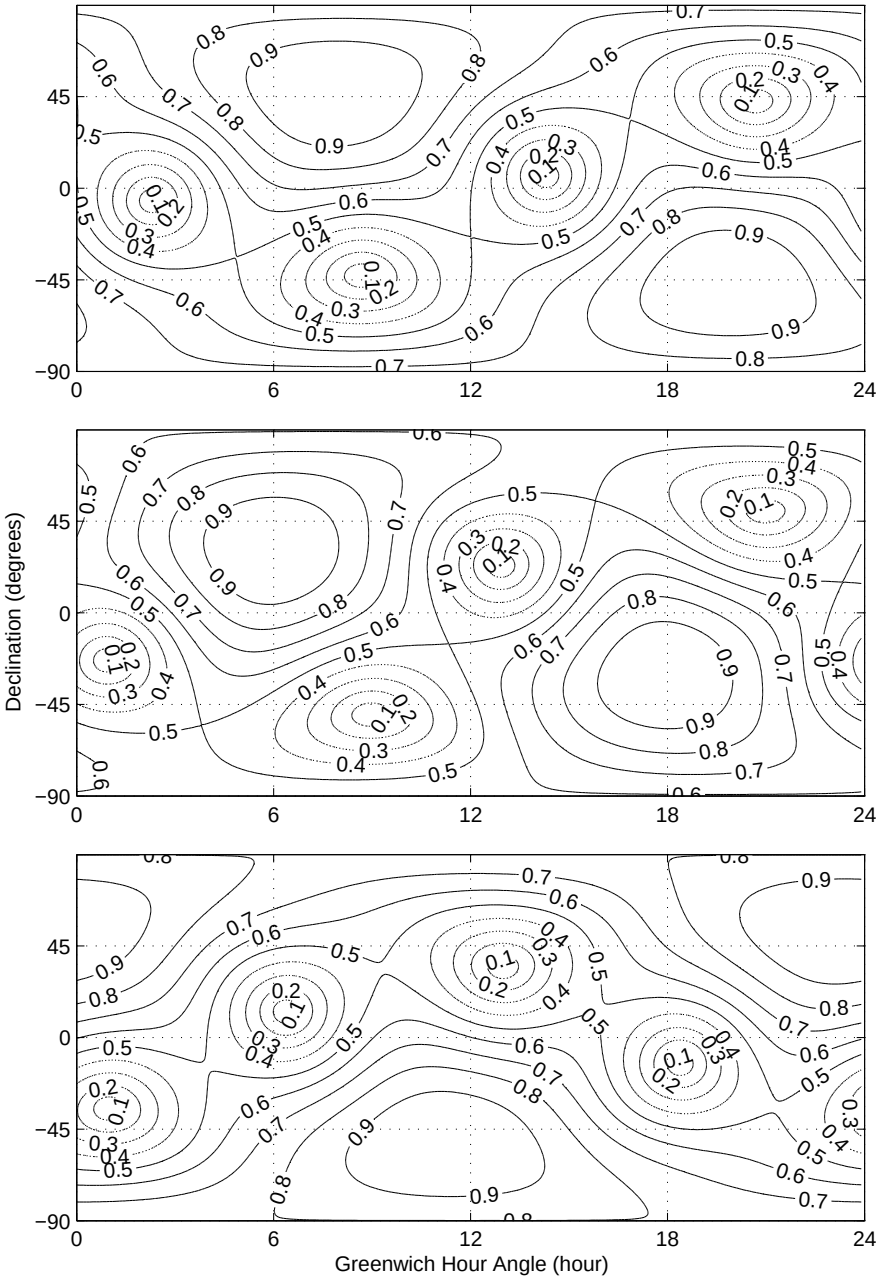

Figure 1. Antenna patterns ($F_+^2 + F_\times^2$) of the Hanford (top), Livingston (middle) and GEO 600 (bottom) detectors. The locations of the maxima and minima in the antenna patterns for Hanford and Livingston are close. However, the antenna pattern for GEO 600 is different from those of the LIGO detectors.

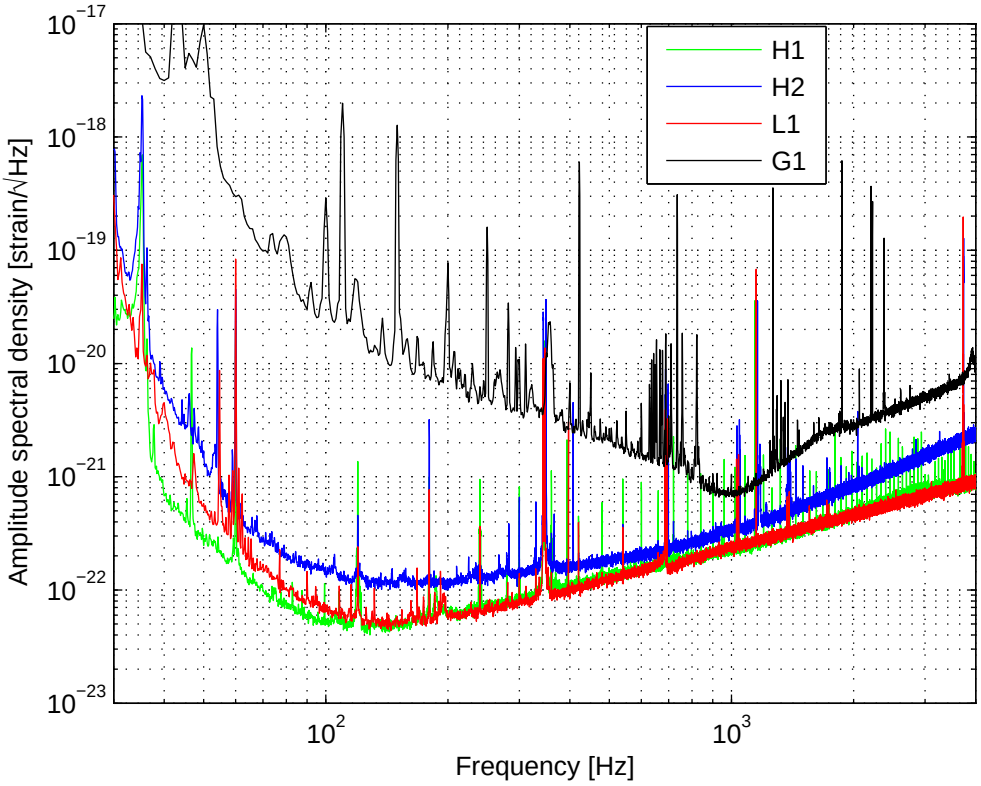

Figure 2. Strain spectral densities of the LIGO Hanford 2 km and 4km detectors (H1, H2) and the LIGO Livingston detector (L1) as well as the GEO 600 detector (G1) during the S4 run. The plotted strain sensitivity curves are the best for the LIGO detectors, obtained on the 26th of February, 2005, for H1 and H2 and the 11th of March, 2005, for L1. The GEO 600 sensitivity curve is typical of the detector's performance during the S4 run.

excess power. Coincident excess power pixels from multiple detectors are then clustered together to form coincident triggers.

The parameters (central time, frequency, duration, bandwidth and significance) of these triggers are then passed on to the CorrPower algorithm. CorrPower calculates the cross-correlation statistic, commonly denoted by r, for the time series data from the different detectors in the following manner:

$$r = \frac{\sum_i (x_i - \bar{x})(y_i - \bar{y})}{\sqrt{\sum_i (x_i - \bar{x})^2}\sqrt{\sum_i (y_i - \bar{y})^2}}, \tag{2}$$

where x and y are the two time series from the detector pairs. This quantity

is calculated for a range of time shifts, corresponding to the range of possible light travel time differences between the detectors for gravitational waves incident from different directions (up to ±10ms for the LIGO detectors). The CorrPower algorithm effectively quantifies how well the data from different detectors match, thereby performing an approximate waveform consistency test.

The maximum value of the r statistic calculated for each pair of detector data streams is then compared with the distribution expected for Gaussian noise, using the Kolmogorov-Smirnoff test to determine the statistical confidence, denoted by Γ, that the two data streams are correlated.

The use of CorrPower in this pipeline is best suited to detectors that are aligned, such as the LIGO detector network. However, GEO 600 is not aligned with the LIGO network. The r statistic can still be used if the source location and signal waveform are known. But, for an all-sky burst search which makes no assumptions about the signal waveform, the detection efficiency of the network may be reduced for the LIGO-GEO network if the r-statistic is applied. Therefore, we chose to apply CorrPower to only the LIGO subset of detectors.

The search pipeline also performs two diagnostic tests on times when H1 and H2 Waveburst triggers are coincident. These two tests take advantage of the fact that H1 and H2 are located in the same site and fully aligned. As a consequence, true gravitational wave signals in H1 and H2 should be strongly correlated and have the same strain amplitude. The pipeline requires,therefore, the H1-H2 triggers to have amplitude ratios greater than 0.5 and less than 2 (This range is determined by studying the amplitude ratios of simulated gravitational-wave signals added to the H1 and H2 data streams). CorrPower also calculates the sign of the cross-correlation between H1 and H2 with no relative time delay, R_0, and demands that this quantity be positive.

3.2. Coherent Waveburst

The cWB pipeline uses the constraint likelihood method for detection of gravitational-wave bursts in interferometric data [17]. The pipeline is designed to work with arbitrary networks of gravitational wave interferometers.

Similar to the WBCP pipeline described in the previous section, the cWB uses wavelet packet transformations to produce TF data. Both pipelines use the same data conditioning algorithms, but the event trigger generators are different. The WBCP pipeline performs TF coincidence of the excess power triggers between the detectors. The cWB pipeline combines the detector data streams into the coherent

maximum likelihood ratio‡.

$$L_m = \sum_{k=1}^{K} (E_k - N_k), \tag{3}$$

where E_k is the normalized energy in the k^{th} detector output stream,

$$E_k = \sum_{ij} \frac{w_k^2(i,j,\tau_k)}{\sigma_k^2(i,j)}, \tag{4}$$

and N_k is the reconstructed energy of the noise in units of the noise RMS,

$$N_k = \sum_{ij} \frac{(w_k(i,j,\tau_k) - \xi_k(i,j,\alpha,\delta))^2}{\sigma_k^2(i,j)}. \tag{5}$$

In the equations above, K is the number of detectors in the network, $w_k[i,j,\tau_k]$ is the sampled detector data delayed by time τ_k (the time i and frequency j indexes run over the TF area occupied by a trigger) and $\sigma_k(i,j)$ is the estimate of the noise standard deviation in each wavelet layer.

The maximum likelihood ratio L_m is the total sum-squared SNR detected in the network. Often N is called the null energy, where the reconstructed gravitational wave signal is subtracted from the data. The estimators of the gravitational wave signal are obtained by the variation of the likelihood ratio (Eq.3) over two unknown functions h_+ and $h_\times$. The maximum likelihood ratio statistic is obtained by substitution of the solutions for the detector responses into Eq. 3.

The cWB pipeline consists of two stages: a) the coherent trigger production stage, when the burst events are identified in the combined data streams and b) the post-production stage, when additional selection cuts are applied to distinguish gravitational wave signals from the background events.

3.2.1. Trigger production

Coherent Waveburst first resamples the calibrated h(t) data streams to 4096 Hz before whitening them in the wavelet (time-frequency) domain. The Meyer wavelet is used to produce TF maps with time resolutions of 1/8, 1/16, 1/32,

‡ The formulation used here defines L_m to be twice the likelihood of the reconstructed signal energy stated in [18].

1/64, 1/128 and 1/256 seconds. The maximum likelihood ratio statistic is then calculated for each TF pixel which effectively combines the TF maps for individual detectors (at the same time resolution) into a single likelihood TF map. Pixels with a likelihood value greater than 12-13 (depending on the time resolution) are selected and clustered to form triggers [18]. The analysis is performed independently for each time resolution, and so may produce a group of triggers at the same time-frequency location. A trigger with the largest value of the likelihood in the group is selected for the post-production analysis.

3.2.2. Post-production analysis

During the cWB post-production analysis we apply additional selection cuts in order to reject instrumental and environmental artifacts. For this we use coherent statistics calculated during the production stage. Empirically we found the following trigger selection cuts which work best for the S4 LIGO-GEO data.

Similar to the likelihood ratio statistic L_m, one can define the sub-network likelihood ratios L_k where the reconstructed SNR for the k^{th} detector is subtracted from L_m,

$$L_k = L_m - (E_k - N_k). \tag{6}$$

In the post-production analysis we require that all L_k are greater than some threshold which effectively removes the single detector glitches.

The likelihood ratio statistic L_m is a quadratic form

$$L_m = \sum_{n,p=1}^{K} L_{np} = \sum_{n,p=1}^{K} C_{np} \langle w_n w_p \rangle, \tag{7}$$

where the sum is taken over all detectors in the network and the coefficients C_{np} depend on the antenna patterns and variance of the detector noise. The $\langle w_n w_p \rangle$ factor is the inner product of the data vectors from the detectors n and p. The diagonal terms of the matrix L_{np} describe the incoherent energy detected by the network. The sum of the off-diagonal terms is the coherent energy E_{coh} which is a measure of the correlation between the detecors.

The second selection cut is based on the rank statistics and the network correlation coefficient

$$cc = \frac{E_{coh}}{N + E_{coh}}. \tag{8}$$

For glitches, typically little coherent energy is detected by the network and the reconstructed detector responses are inconsistent with the detector outputs which result in a large null energy: $E_{coh} < N$ and $cc \ll 1$. For a strong gravitational wave signal, we expect $E_{coh} > N$ and the value of cc to be close to unity. We define the effective rank SNR as

$$\rho_{\rm eff} = \left(\frac{1}{K} \sum_{k=1}^{K} \rho_k \right)^{cc}, \tag{9}$$

where ρ_k is the non-parametric signal-to-noise ratio for each detector based on rank statistic. The ρ_k is a robust measure of the SNR of detected events in the case of non-Gaussian detector noise [24]. We place a threshold on $\rho_{\rm eff}$ to achieve the false alarm rate desired for the analysis.

4. Data Quality

Spurious excitations caused by environmental and instrumental noise increase the number of background triggers in gravitational-wave burst searches. Periods when there are detector hardware problems or when the ambient environmental noise level is elevated are flagged and excluded from the analysis. These *data quality flags* are derived from studies of diagnostic channels and from entries made in the electronic logbook by interferometer operators and scientists on duty that indicate periods of anomalous behaviour in the detector.

Applying data quality flags and vetoes reduces the detectors' observation times. To maximise our chances of detecting a gravitational-wave burst, we must balance this loss against the effectiveness for removing background triggers from the analysis. The data quality flags and vetoes for the LIGO and GEO detectors are outlined below. Out of the 334 hours of quadruple coincidence observation time, 259 hours remained after excluding periods flagged by the data quality flags detailed below.

4.1. GEO 600

4.1.1. Data quality flags

GEO 600 data quality flags include periods when the data acquisition system is saturated (overflow) and when the χ^2 value is too high, as explained below.

The GEO 600 data stream is calibrated into a time series representing the equivalent gravitational-wave strain at each sample. The GEO 600 calibration process determines if the noise, as measured by the acquired data, is close to that expected from the optical transfer function by using the χ^2 statistic [21]. If the χ^2 values are too high, it means that the calibration is not valid. Therefore, the χ^2 values from the calibration process are an indicator of data quality.

4.1.2. Excess glitches

During the first 10 days of the S4 run, one of the suspended GEO components came into contact with a nearby support structure. This caused GEO data to be glitching excessively between the 22nd of February and the 4th of March, 2005. The glitch rate fluctuated dramatically over this period because the distance between the component and the support structure changed as a function of temperature. Given the large variability in the glitch rate (about one order of magnitude on a timescale of hours), we decided to exclude this period from this analysis.

4.2. LIGO

The data quality selection and auxiliary-channel vetoes used with the LIGO detectors are explained in more detail in [8]. Data segments are excluded from the analysis if one of the following occurs:

(i) calibration line injections are not present;
(ii) wind speed at the site is greater than 35 mph;
(iii) seismic activity between 0.4 and 2.4 Hz is seven times the median level;
(iv) an analog-digital-converter (ADC) for one of the two Hanford detectors suffers a data overflow;
(v) the stored light in the arm cavities dips suddenly by 5% or more;

In addition to the exclusion of data segments, triggers attributed to short-duration instrumental or environmental artifacts are excluded from the analysis. This is done by applying vetoes based on triggers generated from auxiliary channels found to be in coincidence with transients in the gravitational wave data, where veto effectiveness (efficiency versus deadtime) is evaluated on background data samples prior to use.

5. Results

Here we present and compare the results of the WBCP and cWB pipelines applied to the LIGO and GEO 600 data.

A total of 259 hours of quadruple coincidence data were processed with both the WBCP and cWB pipelines to produce lists of coincident triggers, each characterised by a central time, duration, central frequency and bandwidth. In addition to these characteristics, each trigger also has an estimated significance with respect to the background noise. Waveburst calculates the overall significance, Z_g, while CorrPower calculates the confidence, Γ. For coherent Waveburst, each trigger is characterised by the likelihood and effective SNR (see equations 6 and 9 respectively). The central frequencies for triggers from both pipelines were restricted to lie between 768 and 2048 Hz. This is because the sensitivity of the GEO 600 detector is closest to the LIGO detectors in this frequency range (see Figure 2). Moreover, the noise of GEO 600 is not very stationary at frequencies below 500 Hz, and many spurious glitches can be observed in the acquired data. CorrPower computes the r statistic over a broader band (64-3152 Hz), using only LIGO data.

For both pipelines, the L1 data are shifted with respect to H1, H2 and G1 data by 100 3.125-second time steps. The applied time shift is sufficiently large that any short gravitational-wave bursts present in the data cannot be observed in coincidence in all detectors. Therefore, we can study the statistics of the noise and tune the thresholds of the pipeline without bias from any possible gravitational wave signals that might be present in the data. The goal of the tuning is to reduce the number of time-shifted coincidences while maintaining high detection efficiency to simulated gravitational wave signals.

The efficiency of the pipeline at detecting gravitational-wave bursts for the selected thresholds is determined by adding into the data simulated gravitational wave signals of various morphologies and amplitudes. For this study, we used sine-Gaussians, sine waves with a Gaussian envelope, given, in the detector frame, by

$$h_+(t) = h(t)\cos 2\psi, \tag{10a}$$

$$h_\times(t) = h(t)\sin 2\psi, \tag{10b}$$

where

$$h(t) = h_0 \sin(2\pi f_0[t - t_0]) \exp[-(2\pi f_0[t - t_0])^2/2Q^2]. \quad (11)$$

Here, the *polarisation angle* ψ is uniformly distributed on $[0, \pi]$, t_0 and h_0 are the peak time and amplitude of the envelope, Q is the width of the envelope, and f_0 is the central frequency of the signal. The antenna pattern for each detector in the network is taken into account before the signal is digitally added to the data stream. The signal strength is parameterised in terms of the root-sum-squared amplitude of signal injected in each interferometer, $h_{\rm rss}$,

$$h_{\rm rss} \equiv \sqrt{\int |h_+(t)|^2 + |h_\times(t)|^2 \, {\rm d}t}. \quad (12)$$

where $h_+(t)$ and $h_\times(t)$ are the strain amplitudes of the plus and cross polarisations of the signal respectively.

The detection efficiency is the fraction of injected signals that produce triggers surviving the selected thresholds for the respective pipeline. We characterise the sensitivity of each pipeline by its $h_{\rm rss}^{50\%}$, which is the $h_{\rm rss}$ at which 50% of the injected signals are observed at the end of the pipeline (detection efficiency).

5.1. Waveburst-CorrPower analysis

For the WBCP pipeline, there are two threshold values to select. The quadruple accidental coincidence rate as a function of the threshold on Waveburst significance is shown in Figure 3. Since the calculation of the r-statistic by CorrPower is computationally expensive and time consuming, we reduce the number of triggers by selecting an initial Waveburst significance threshold of $Z_g > 5.05$, for a false alarm rate of approximately 2×10^{-5} Hz.

The CorrPower confidence, Γ, is then calculated for each surviving trigger. A scatter plot of Γ versus Z_g for these triggers can be seen in figure 4. Note that, while all zero-lag triggers have Γ values less than 4, there is a single background trigger with an extremely large value of Γ and a low Z_g. This trigger is caused by a non-stationary instrumental line that survives the data whitening procedure generating a large correlation between two detectors.

Table 1 shows the number of accidental background coincidences and the $h_{\rm rss}^{50\%}$ values for sine-Gaussian injections of different central frequencies for several trial values of the threshold on Γ: $\Gamma > 0$ (CorrPower not used), $\Gamma > 3$ and $\Gamma > 4$. We note that the $h_{\rm rss}^{50\%}$ values for a threshold of $\Gamma > 4$ are only a few percent worse than those for $\Gamma > 3$, while the number of accidental coincidences is reduced from

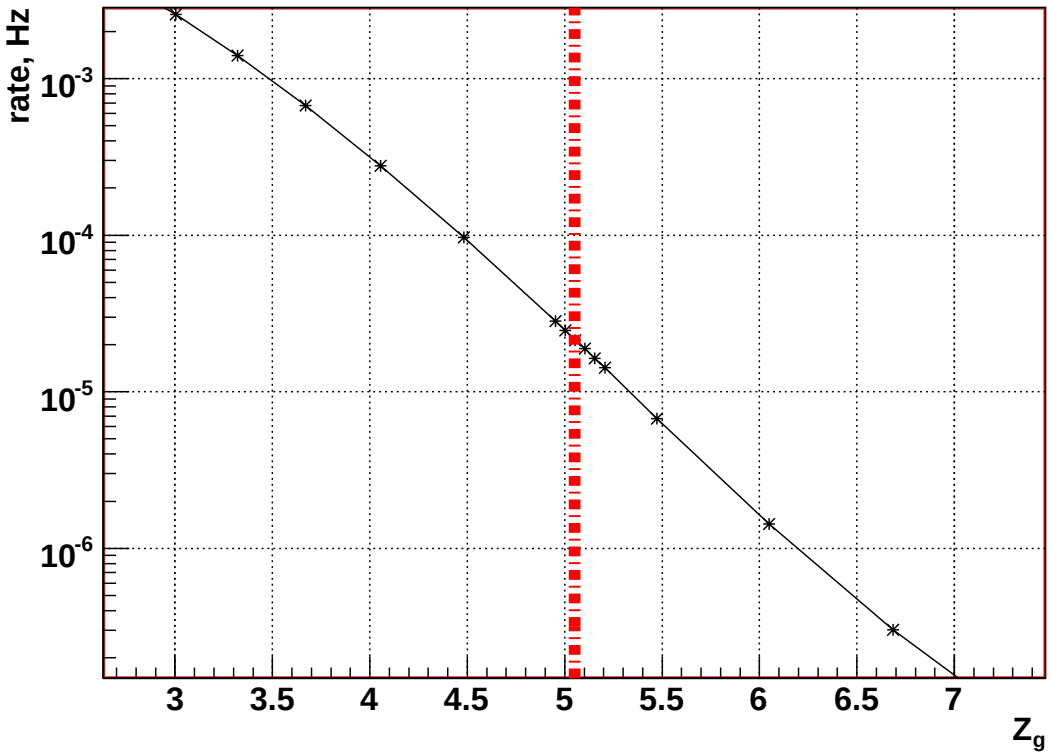

Figure 3. Quadruple coincidence rate as a function of the threshold on the Waveburst significance, Z_g. The threshold used for this analysis is indicated by the dotted line. [Figure not final. Line to be removed, plot to be reformatted to match others]

4 to 1. With the implied reduction rate in false alarm rate in mind, we choose the CorrPower threshold of $\Gamma > 4$. The fraction of sine-Gaussian signals detected above threshold (detection efficiency) as a function of injected $h_{\rm rss}$ is shown in figure 5. We plot the measured $h_{\rm rss}^{50\%}$ for the different central frequencies of the injected sine-Gaussian signals for our threshold choices of $Z_g > 5.05$ and $\Gamma > 4$ in Figure 8.

5.2. Coherent Waveburst analysis

For cWB, the tuning strategy is to set thresholds such that no background triggers are observed. We first require that L_k for all three-detector combinations in the

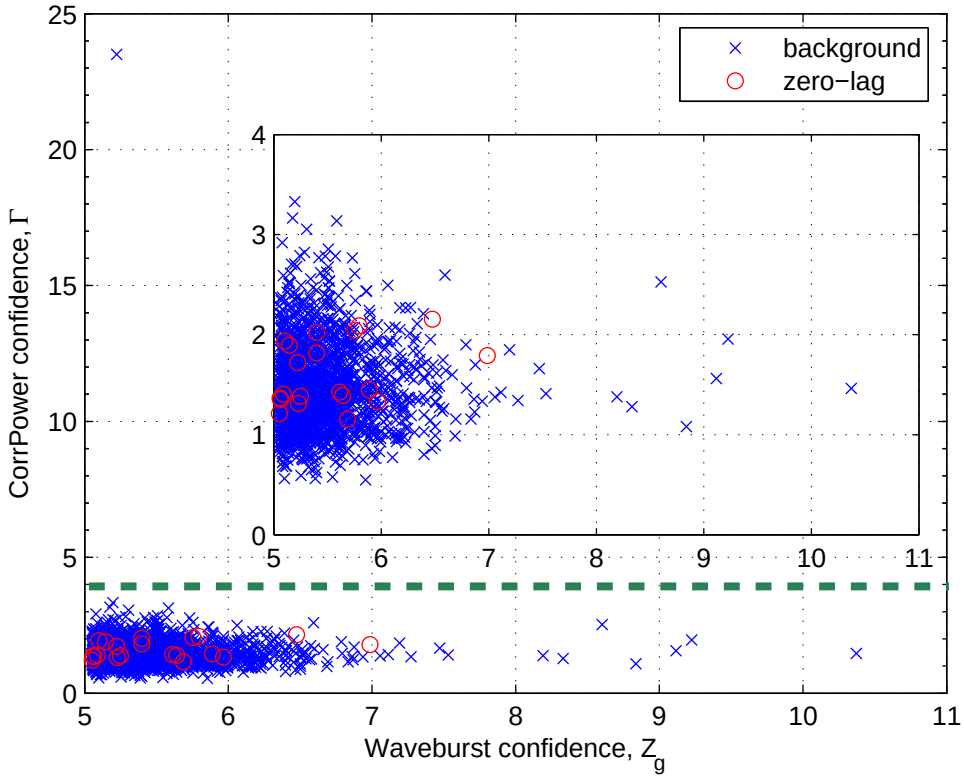

Figure 4. Scatterplot of r-statistic confidence, Γ versus Waveburst Z_g. Background triggers from time shifts are indicated by "x", while zero-lag triggers (potential gravitational-wave candidates) are indicated by "o". The insert is an expanded view of the same plot for Γ values of 0 to 4. The dashed green line indicates the Γ threshold chosen for this analysis.

network be greater than 36. We then set the effective SNR threshold high enough to eliminate all remaining background triggers. Figure 6 shows the quadruple coincidence rate as a function of effective SNR, ρ_{eff}. We set the effective SNR threshold at 3.4.

To determine the detection efficiency, we then inject sine-Gaussian burst signals into the data and determine the fraction of injections detected for the selected effective SNR and likelihood thresholds. Figure 7 plots the detection efficiency as a function of the $h_{\rm rss}$ of the injected sine-Gaussians.

Table 1. Table of accidental coincidences and $h_{\rm rss}^{50\%}$ as a function of Γ

Γ threshold	accidental coincidences	Frequency [Hz]	$h_{\rm rss}^{50\%}$ [$\times 10^{-21}$ Hz$^{-1/2}$]
0	3335	849	5.9
		1053	6.4
		1616	12.0
3	4	849	5.9
		1053	6.6
		1616	12.0
4	1	849	6.2
		1053	6.7
		1616	12.2

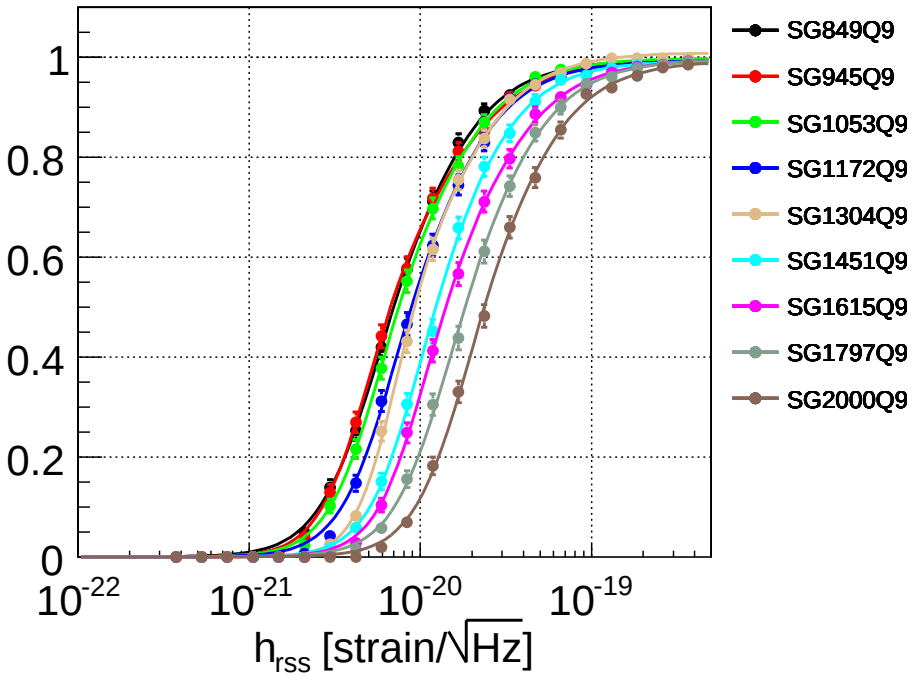

Figure 5. Detection efficiency for WBCP pipeline for sine-Gaussians with different central frequencies. [Figure not final. Plot to be reformatted to match other figures]

5.3. Zero-lag observations and efficiency comparison

With the thresholds chosen using the time-shifted analysis detailed in the previous two subsections, a search for gravitational waves is performed on LIGO-GEO data

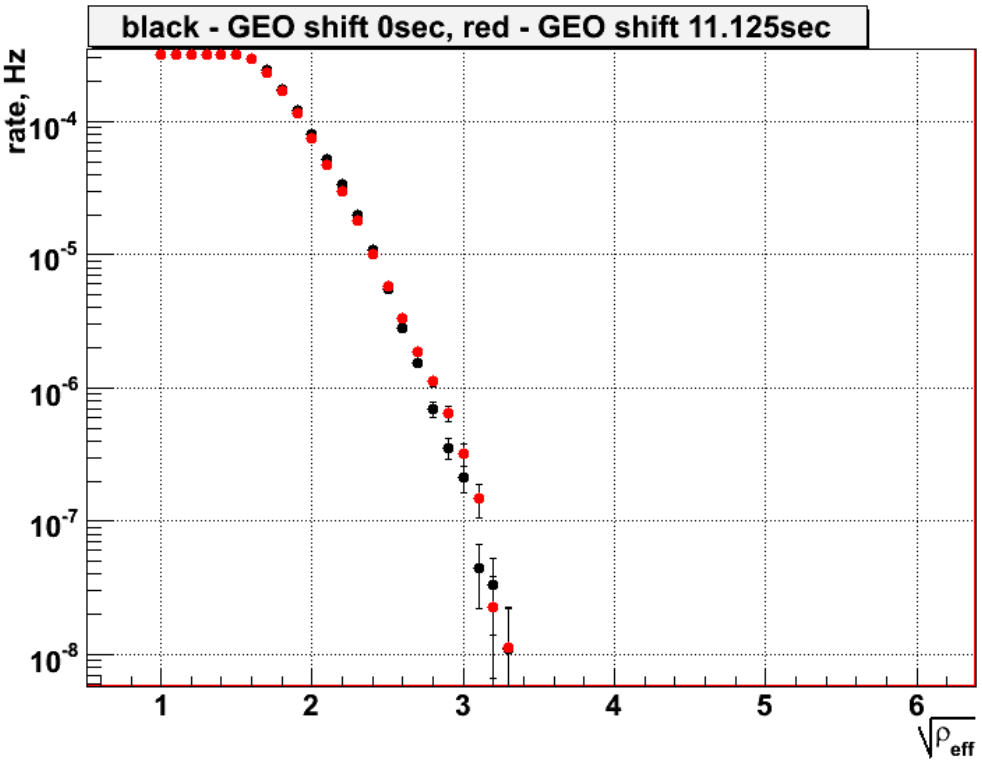

Figure 6. Rate of accidental coincidences as a function of effective SNR for the cWB pipeline. The L1 data is shifted in 100 discrete time steps from -156.25 to 156.25 seconds and, for each threshold value of ρ_{eff}, the accidental coincidence rate is calculated by taking an average over all 100 time shifts (black dots). As a consistency test, the accidental coincidence rate is determined for the same set of L1 time shifts but with a fixed 11.125 second offset applied to G1 data. The accidental coincidence distribution with the 11.125-second offset (red dots) is very similar to that without any offset applied to G1 data. [Figure not final. X-axis mislabelled, plot to be reformatted to match other figures]

between 768 and 2048 Hz with no time shift applied (zero-lag). No coincidences are observed above the chosen thresholds for either pipeline.

The next step is to compare the sensitivities of the two pipelines, which we characterised by the $h_{\rm rss}^{50\%}$ values (the minimum signal amplitude required for a detection efficiency of at least 50%). The $h_{\rm rss}^{50i\%}$ values for the two pipelines used on the LIGO-GEO S4 data set are given in Table 2 and plotted against the strain spectral densities of the detectors in figure 8. We note that the $h_{\rm rss}^{50\%}$ values obtained for the cWB pipeline are $30-50\%$ lower than those of the WBCP pipeline. As

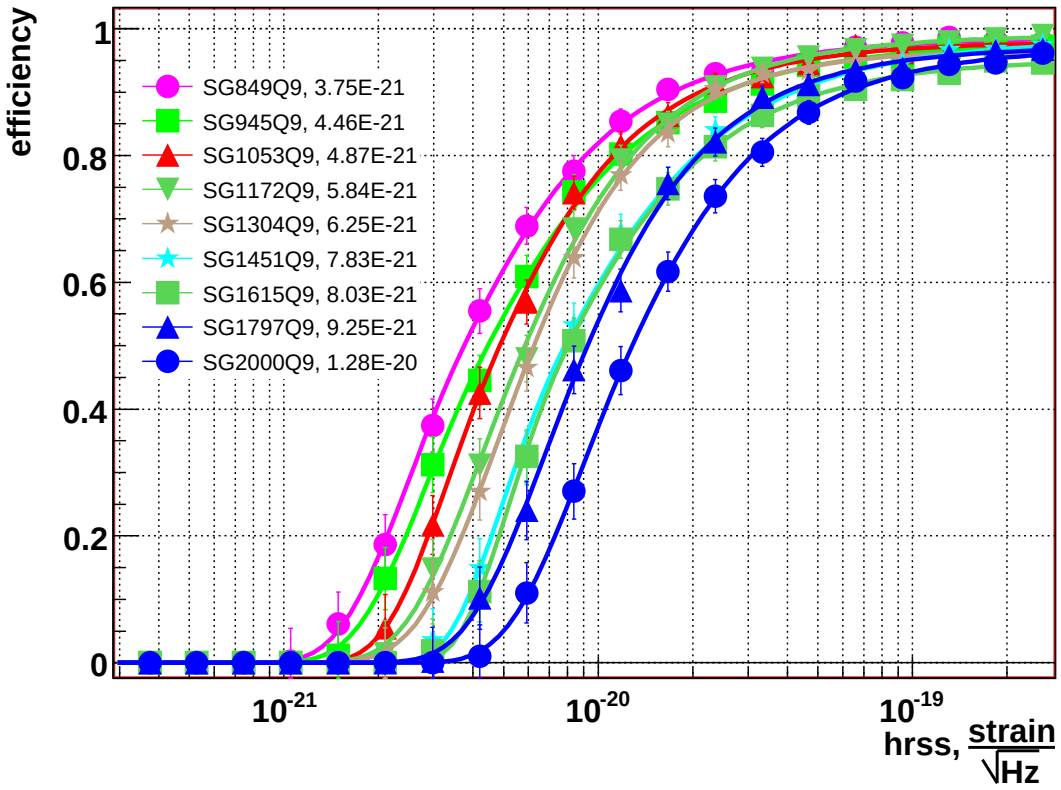

Figure 7. Detection efficiency of the coherent Waveburst pipeline for various sine-Gaussian simulated gravitational-wave bursts, as a function of the signal amplitude (defined by equation 11). The legend indicates the central frequency (Hz) of the injected signal and the $h_{\rm rss}^{50\%}$ ($\mathrm{Hz}^{-1/2}$) sensitivity of the pipeline. [Figure not final. Plot to be reformatted to match other figures]

desired, the $h_{\rm rss}^{50\%}$ values for the cWB pipeline are also better than those for the same signals at these frequencies for a WBCP gravitational-wave burst search using only LIGO S4 data (4.5×10^{-21} $\mathrm{Hz}^{-1/2}$ at 849 Hz and 6.3×10^{-21} $\mathrm{Hz}^{-1/2}$ at 1053 Hz)§ [8].

§ This search was performed in a different frequency range, 64 to 1600 Hz, from that reported here.

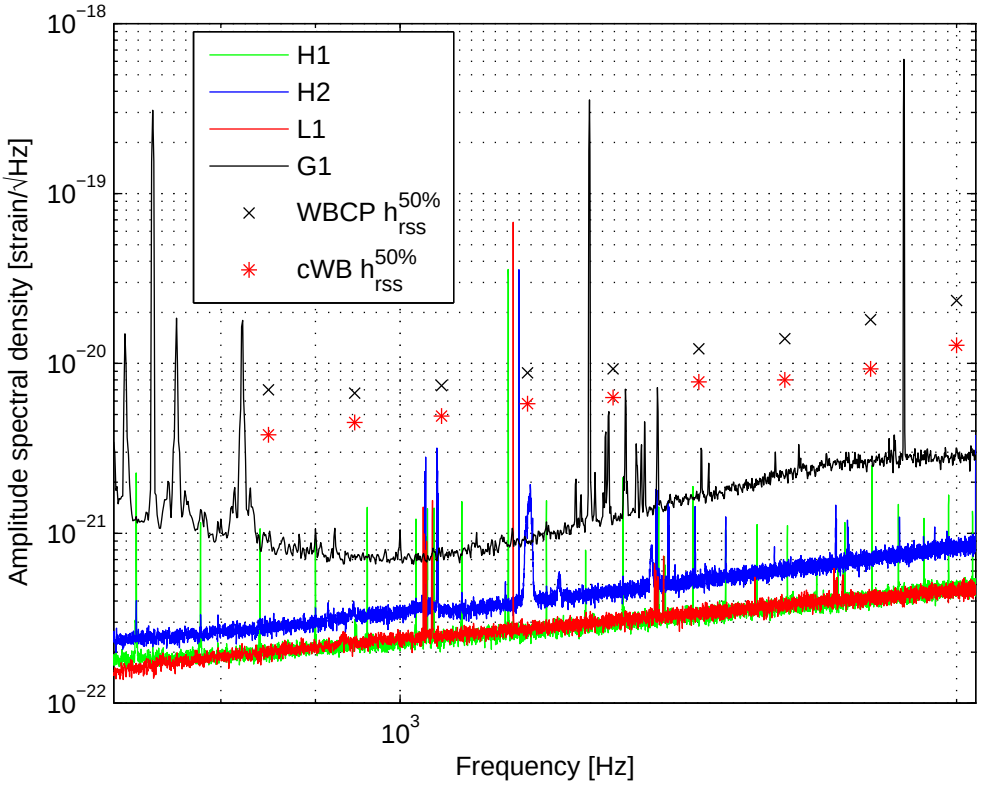

Figure 8. The $h_{\rm rss}^{50\%}$ values for Waveburst-CorrPower ('x' markers) and coherent Waveburst ('*' markers) pipelines for sine-Gaussians of different central frequencies. Coherent Waveburst is sensitive to gravitational wave signals with amplitudes $30-50\%$ lower than those detectable by Waveburst-CorrPower.

6. Discussion

The first joint search for gravitational-wave bursts using the LIGO and GEO 600 detectors has been presented. The search was performed using two pipelines, WBCP and cWB, and targeted signals in the frequency range 768-2048 Hz. No candidate gravitational wave signals have been identified.

The detection efficiencies of the two pipelines to sine-Gaussians have been compared. The CWB pipeline has $h_{rss}^{50\%}$ values $30-50\%$ lower than those of the WBCP pipeline. These improved detection efficiencies are also better than those obtained for the all-sky burst search using only LIGO S4 data and the WBCP pipeline [8]. One should note, however, that this search was performed at a lower frequency range (64 to 1600 Hz) from the LIGO-GEO analysis reported in this

Table 2. Table of $h_{\rm rss}^{50\%}$ as a function of sine-Gaussian central frequencies

sine Gaussian	$h_{\rm rss}^{50\%}$ [$\times 10^{-21}$ Hz$^{-1/2}$]	
central frequency [Hz]	Waveburst-CorrPower	coherent Waveburst
849	7.0	3.8
945	6.7	4.5
1053	7.4	4.9
1172	8.8	5.8
1304	9.3	6.3
1451	12.2	7.8
1615	14.0	8.0
1797	18.1	9.3
2000	23.5	12.8

article. Nonetheless, these results show that, for WBCP, the detection efficiency is limited by the least sensitive detector when applied to a network of detectors with different antenna patterns and noise levels. This is because WBCP requires that excess power be observed in coincidence by all detectors in the network. On the other hand, the cWB pipeline naturally includes detectors of different sensitivities by weighting the data with the antenna patterns and noise. Therefore, the detection efficiency of the network is not limited by the least sensitive detector.

Acknowledgments

The authors gratefully acknowledge the support of the United States National Science Foundation for the construction and operation of the LIGO Laboratory and the Science and Technology Facilities Council of the United Kingdom, the Max-Planck-Society, and the State of Niedersachsen/Germany for support of the construction and operation of the GEO600 detector. The authors also gratefully acknowledge the support of the research by these agencies and by the Australian Research Council, the Council of Scientific and Industrial Research of India, the Istituto Nazionale di Fisica Nucleare of Italy, the Spanish Ministerio de Educación y Ciencia, the Conselleria d'Economia, Hisenda i Innovació of the Govern de les Illes Balears, the Scottish Funding Council, the Scottish Universities Physics Alliance, The National Aeronautics and Space Administration, the Carnegie Trust,

the Leverhulme Trust, the David and Lucile Packard Foundation, the Research Corporation, and the Alfred P. Sloan Foundation. This document has been assigned LIGO Laboratory document number LIGO-P0800008-00-Z.

References

[1] D. Sigg (for the LIGO Scientific Collaboration), *Class. Quantum Grav.* **23** (2006) S51–6
[2] H. Lueck *et al.*, *Class. Quantum Grav.* **23** (2006) S71–S78.
[3] F. Acernese *et al*, *Class. Quantum Grav.* **23** (2006) S63–9.
[4] M. Ando and the TAMA Collaboration, *Class. Quantum Grav.* **22** (2005) S881–9.
[5] B. Abbott *et al.*, *Phys. Rev. D* **69** (2004) 102001.
[6] B. Abbott *et al.*, *Phys. Rev. D* **72** (2005) 062001.
[7] B. Abbott *et al.*, *Class. Quantum Grav.* **23** (2006) S29–39.
[8] B. Abbott *et al.*, *Class. Quantum Grav.* **24** (2007) 5343–5369.
[9] B. Abbott *et al.*, *Phys. Rev. D* **72**, (2005) 122004.
[10] S. Klimenko and G. Mitselmakher, *Class. Quantum Grav.* **21** (2004) S1819-1830.
[11] L. Cadonati and S. Márka, *Class. Quantum Grav.* **22** (2005) S1159-67.
[12] L. Cadonati, *Class. Quantum Grav.* **21** (2004) S1695-703.
[13] Y. Guersel and M. Tinto, *Phys. Rev. D* **40** (1989) 3884–3939.
[14] E.E. Flanagan and S.A. Hughes, *Phys. Rev. D* **57**, (1997) 4566–4587.
[15] L. Wen L and B. Schutz, *Class. Quantum Grav.* **22** (2005) S1321–35.
[16] S. Chatterji, A. Lazzarini, L. Stein, P.J. Sutton, A. Searle and M. Tinto, *Phys. Rev. D* **74** (2006) 082005.
[17] S. Klimenko, S. Mohanty, M. Rakhmanov and G. Mitselmakher, *Phys. Rev. D* **72** (2005) 122002.
[18] S.Klimenko, I.Yakushin, A.Mercer, G.Mitselmakher arXiv: 0802.3232v1 [gr- qc] 21 Feb 2008; submitted to *Class. Quantum Grav.*.
[19] S. Hild for the LIGO Scientific Collaboration, *Class. Quantum Grav.* **23** (2006) S643-S651.
[20] M. Hewitson, H. Grote, S. Hild, H. Lueck, P. Ajith, J.R. Smith, K.A. Strain, B. Willke and G. Woan, *Class. Quantum Grav.* **22** (2005) 4253-4261.
[21] S. Hild, H. Grote, J.R. Smith, M. Hewitson for the GEO 600-team, *J. Phys.: Conf. Ser.* **32** (2006) 66-73.
[22] I. Daubechies 1992, *Ten lectures on wavelets*. Philadelphia, SIAM
[23] W.G. Andersion, P.R. Brady, J.D.E. Creighton, and E.E. Flanagan, *Phys. Rev. D* **63** (2001) 042003.
[24] S. Klimenko, I. Yakushin, M. Rakhmanov and G. Mitselmakher, *Class. Quant. Grav.*, **21** (2004) S1685-S1694.